



A primate temporal cortex–zona incerta pathway for novelty seeking

Takaya Ogasawara¹✉, Fatih Sogukpinar^{2,6}, Kaining Zhang^{1,3,6}, Yang-Yang Feng³, Julia Pai¹, Ahmad Jezzini¹ and Ilya E. Monosov^{1,2,3,4,5}✉

Primates interact with the world by exploring visual objects; they seek opportunities to view novel objects even when these have no extrinsic reward value. How the brain controls this novelty seeking is unknown. Here we show that novelty seeking in monkeys is regulated by the zona incerta (ZI). As monkeys made eye movements to familiar objects to trigger an opportunity to view novel objects, many ZI neurons were preferentially activated by predictions of novel objects before the gaze shift. Low-intensity ZI stimulation facilitated gaze shifts, whereas ZI inactivation reduced novelty seeking. ZI-dependent novelty seeking was not regulated by neurons in the lateral habenula or by many dopamine neurons in the substantia nigra, traditionally associated with reward seeking. But the anterior ventral medial temporal cortex, an area important for object vision and memory, was a prominent source of novelty predictions. These data uncover a functional pathway in the primate brain that regulates novelty seeking.

Humans and other primates express strong desires to inspect novel objects^{1–6}. However, the neuronal mechanisms underlying novelty seeking are poorly understood. A dominant theory suggests that neurons that process reward, particularly dopamine (DA) neurons that signal reward-prediction errors^{7–9}, also process novelty as a reward. This notion is supported by theoretical work^{10–13} inspired by neuroimaging findings that when subjects are shown novel objects selective changes in blood oxygenation are detected in and around the substantia nigra (SN)^{14,15}.

There is strong evidence that DA neuron activity reflects the subjective value of primary, appetitive rewards^{7,16–19}, and can also signal more abstract forms of reward, such as preferences for obtaining information about upcoming uncertain rewards²⁰ and for social interactions^{21,22}. Whether DA neurons also encode the preference for novelty for its own sake remains unknown. Similarly, it is unclear whether activity of DA neurons, or other neurons, predicts future novelty because studies of neural response to the presentation of novel or familiar objects^{23,24} did not assess responses to upcoming, predicted novelty.

Other theories of novelty seeking have also arisen from the efforts of artificial learning researchers, for example aiming to construct ‘self-evolving’ agents^{1,25–27}. They propose that novelty seeking could be controlled relatively independently from reward seeking which has advantages. For example, it could solve the ‘sparse-reward learning problem’ by encouraging agents to seek novelty and explore it even when there are no immediate rewards to be obtained¹. Consistent with this idea, several studies suggest that novelty seeking and reward seeking may be behaviorally dissociable. For example, human infants, adults and many animals exhibit novelty-seeking actions that are not related to reward expectancy¹. To date, the question has remained whether reward prediction and novelty seeking are dissociable at the level of neural circuits.

Here we show, using electrophysiology, causal manipulations of neuronal activity, and detailed analyses of primate behavior,

that the ZI controls novelty seeking; that is, the seeking of never-before-seen objects.

Studies in rodents have illuminated the role of the ZI in integrating wide-ranging higher-order cortical inputs^{28,29} to directly control various behaviors^{30–33} and internal states, including those related to arousal and changes in exploratory and motivated behaviors in response to the presence of salient stimuli^{34,35}. In primates, the ZI has a prominent projection to the superior colliculus³⁶, a key controller of gaze and attention³⁷. However, the functional role of the ZI in primate behavior has been unclear. Our data show that the primate ZI is crucial for novelty-seeking gaze behavior, by helping to transform higher-order signals about predictions of future object novelty into action. Further experiments showed that novelty seeking was behaviorally and neuronally dissociable from reward-prediction errors at the level of the habenula–DA pathway. Putative dopamine neurons in the SN pars compacta (SNc) and neurons in the lateral habenula (LHb) were relatively inactive during novelty seeking when novel objects did not predict future rewards or reward learning. Instead, high channel-count electrophysiological experiments identified the anterior ventral medial temporal cortex (AVMTC), a brain region involved in visual processing and memory^{38,39}, as a prominent source of novelty predictions well suited to mediate novelty seeking. These findings are consistent with models that posit that reward prediction and novelty seeking can be controlled by multiple motivational systems.

Results

Monkeys seek novel objects that do not have extrinsic reward value. We trained monkeys to perform a behavioral task that included novelty-seeking trials and novelty-inspecting trials. In novelty-seeking trials, monkeys could choose to shift their gaze to a familiar peripheral fractal object to gain the opportunity to view a novel fractal object (Fig. 1a, top). In novelty-inspecting trials, a novel object appeared immediately at the time of fractal onset.

¹Department of Neuroscience, Washington University School of Medicine, St. Louis, MO, USA. ²Department of Electrical Engineering, Washington University, St. Louis, MO, USA. ³Department of Biomedical Engineering, Washington University, St. Louis, MO, USA. ⁴Department of Neurosurgery School of Medicine, Washington University, St. Louis, MO, USA. ⁵Pain Center, Washington University School of Medicine, St. Louis, MO, USA. ⁶These authors contributed equally: F. Sogukpinar and K. Zhang. ✉e-mail: takaya.ogasawara@wustl.edu; ilya.monosov@gmail.com

In all trials, the amount and rate of reward were not affected by whether the monkeys looked at the fractal objects, and the novel objects could not be used to maximize reward on subsequent trials (Fig. 1a, bottom).

In novelty-seeking trials, one of two novelty-predicting (NP) visual fractal objects was presented on either the left or the right side of the screen. After the fixation point disappeared ('go' signal), the monkey was free to gaze in any manner it chose ('free viewing'). Gazing at a NP object during free viewing caused it to be replaced by a novel object (Fig. 1a, top, NP trials). Thus, the earlier the monkeys shifted their gaze to the NP object, the earlier they could gaze at the novel object. On other control trials, one of two familiarity-predicting (FP) objects was presented. Gazing at a FP object during free viewing caused it to be replaced by a familiar object (Fig. 1a, top, FP trials). The monkeys were extensively familiarized with the NP and FP objects during training, and were thus able to learn that NP objects were consistently associated with access to novel objects and that FP objects were associated with access to familiar objects. This design enabled us to study the monkeys' motivation to obtain novel objects by comparing how rapidly they shifted their gaze to the NP versus FP objects, analogous to conventional measures of gaze-mediated reward-seeking motivation which compare how rapidly monkeys shift their gaze to objects that deliver large or small rewards^{40,41}.

In novelty-inspecting trials, a novel object appeared immediately following fixation and remained on until reward was delivered (Fig. 1a, bottom, N trials); analogous control familiarity-inspecting trials presented a familiar object (Fig. 1a, bottom, F trials). All four trial types were interleaved and hence were not fully predictable.

Novelty-seeking trials allowed us to study the prediction and seeking of future novel objects, whereas novelty-inspecting trials allowed us to study neural and behavioral responses to the unpredictable onset of novel objects themselves.

Previous studies showed that monkeys gaze at novel objects more than familiar objects^{3,42}. However, it has been mostly unclear whether or not animals are motivated by the promise of novel objects that are not yet available, an important form of novelty

seeking and prediction⁴³. We found that in novelty-seeking trials, monkeys displayed stable novelty-seeking behavior. All four monkeys were faster to shift their gaze onto familiar NP objects (fractal object acquisition time) that yielded novel objects than onto familiar FP objects that yielded familiar objects (Fig. 1b, left and Supplementary Fig. 1a, left). In novelty-inspecting and familiarity-inspecting trials, monkeys acquired the peripheral object faster when it was novel than when it was familiar (Fig. 1b, left) and generally gazed at novel objects more than familiar objects during 'free viewing' (Fig. 1b, right and Supplementary Fig. 1a, right and b). Hence, our task allowed us to show that monkeys predicted, and were motivated to seek, novel objects (Fig. 1b, left). This behavioral bias was present even though the monkeys always received the same juice reward, and the behavioral differences across NP and FP trials could not be attributed to differences in reward expectancy. To quantify the strength of novelty-seeking behavior, we computed a novelty bias index that quantifies the novelty-related differences in object acquisition times in trials with novel objects versus trials without novel objects. This measure isolated the influence of novelty on motivation (Fig. 1c, positive values indicate positive novelty bias). All monkeys displayed the motivation to seek novel objects (Fig. 1c).

Finally, we assessed whether the response-time biases (Fig. 1b,c), which often reflect the level of motivation^{40,44}, reflected the monkeys' preferences for novelty. In a 'novelty choice' task in which monkeys could choose between obtaining a novel or familiar object on each trial (Supplementary Fig. 2), monkeys preferred to receive novel objects (Fig. 1d), consistent with their response-time biases in novelty-seeking trials.

Single ZI neuron signals novelty predictions. Next, we sought to uncover the neural mechanisms that underlie novelty seeking. To target the ZI and other brain regions, we used a combination of previously outlined electrophysiological and imaging methods (Methods and Supplementary Fig. 3).

Many neurons in the ZI encoded the opportunity to experience novel objects. One example ZI neuron is shown in Fig. 1e. This

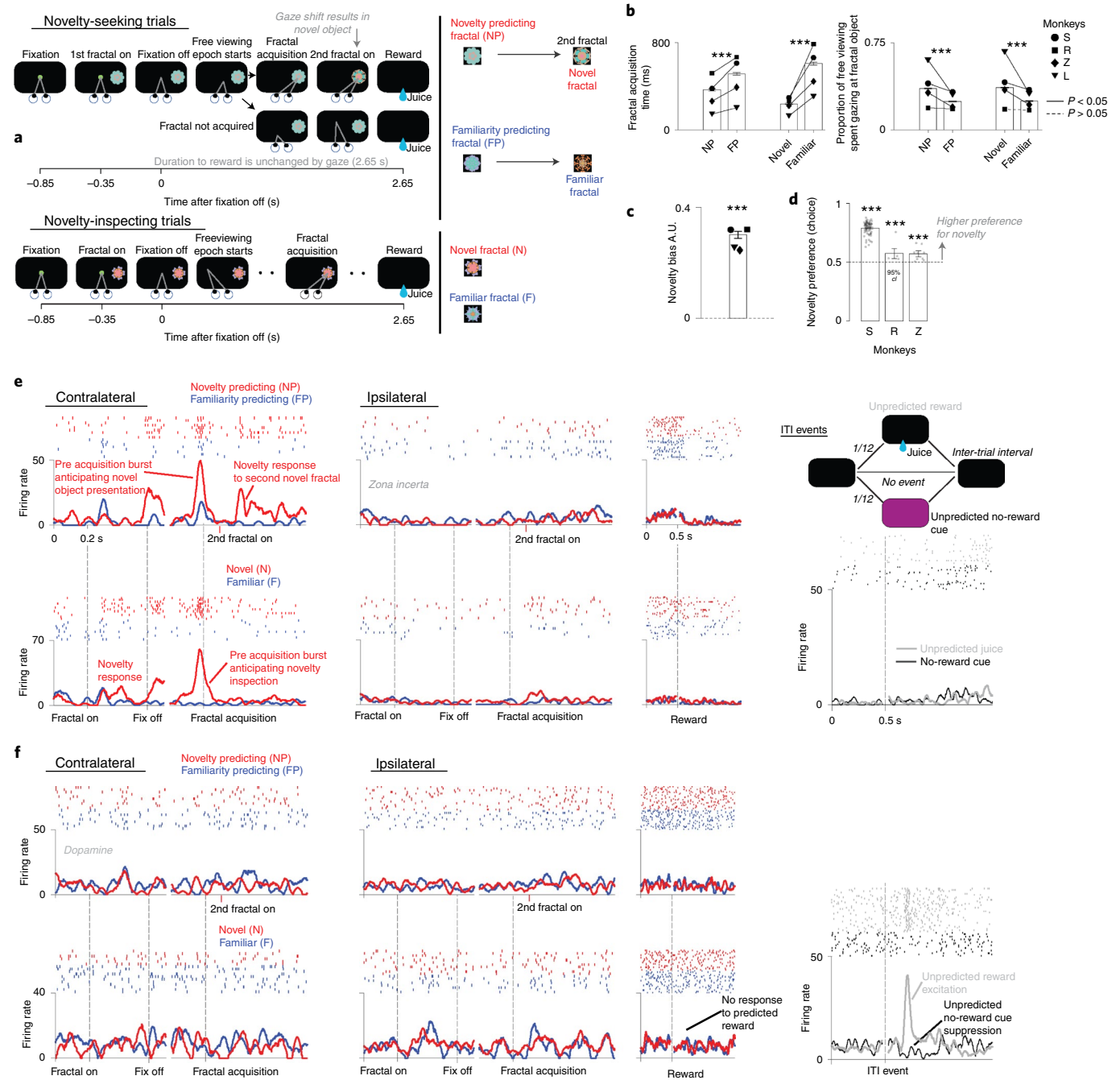
Fig. 1 | Behavior and single neurons' activities during novelty seeking. **a**, Behavioral task diagram. **b**, Fractal object acquisition time (left). Every monkey was faster to saccade to familiar objects that yielded novel objects as compared to those that yielded familiar objects (novelty-predicting (NP) objects versus familiarity-predicting (FP) objects). Also, during 'free viewing' monkeys gazed at novel objects more than familiar objects (right). Bars indicate mean fractal object acquisition time (left) and mean proportion of free viewing spent gazing at object (right) across single trials from the recording sessions ($n = 252$ sessions). Symbols indicate data for each monkey separately ($n = 61$ sessions in monkey S, 123 sessions in monkey R, 42 sessions in monkey Z and 26 sessions in monkey L). Error bars indicate s.e.m. across all single trials (left: $n = 4,472$ trials in NP trials, 4,239 trials in FP trials, 4,399 trials in novel trials and 4,129 trials in familiar trials; right: $n = 3,908$ trials in NP trials, 3,392 trials in FP trials, 4,157 trials in novel trials and 3,135 trials in familiar trials). Asterisks indicate significant differences ($***P < 0.001$, left: $P_{(NP \text{ versus FP})} = 8.3 \times 10^{-40}$, $P_{(novel \text{ versus familiar})} = 2.4 \times 10^{-170}$, right: $P_{(NP \text{ versus FP})} = 5.7 \times 10^{-62}$, $P_{(novel \text{ versus familiar})} = 7.3 \times 10^{-60}$, Wilcoxon rank-sum test). Solid lines indicate significant differences for data for each monkey ($P < 0.05$). Left: $P_{(NP \text{ versus FP})} = 2.5 \times 10^{-18}$ in monkey S, 1.2×10^{-10} in monkey R, 1.8×10^{-7} in monkey Z, 1.3×10^{-21} in monkey L, $P_{(novel \text{ versus familiar})} = 5.8 \times 10^{-38}$ in monkey S, 1.9×10^{-95} in monkey R, 2.9×10^{-4} in monkey Z, 1.1×10^{-53} in monkey L. Right: $P_{(NP \text{ versus FP})} = 3.6 \times 10^{-7}$ in monkey S, 0.010 in monkey R, 4.7×10^{-18} in monkey Z, 9.0×10^{-62} in monkey L, $P_{(novel \text{ versus familiar})} = 2.4 \times 10^{-5}$ in monkey S, 0.067 in monkey R, 4.4×10^{-16} in monkey Z, 2.3×10^{-82} in monkey L (Wilcoxon rank-sum test). **c**, Average of novelty bias index across all sessions. AU, arbitrary units. Each symbol indicates mean bias for each monkey. The number of sessions was the same as in **b**. Error bar: s.e.m. across all sessions. Asterisks indicate significant difference from zero ($***P = 2.0 \times 10^{-39}$, Wilcoxon signed-rank test). **d**, Novelty preference across all trials for each monkey. Preference was assessed in a novelty-choice task in which monkeys chose among NP and FP objects (Supplementary Fig. 2). Each bar indicates each monkey's choice rate of NP objects over FP objects across all single trials ($n = 11,102$ trials in monkey S, 557 trials in monkey R and 1,510 trials in monkey Z). Each dot indicates single session's choice rate ($n = 68$ sessions in monkey S, four sessions in monkey R and nine sessions in monkey Z). Error bars indicate 95% confidence interval across all single trials (Clopper-Pearson method). Asterisks indicate a significant deviation from 0.5 (chance). $***P < 1.0 \times 10^{-8}$ in monkey S, $P = 6.9 \times 10^{-4}$ in monkey R and $P = 4.0 \times 10^{-8}$ in monkey Z (binomial test). **e,f**, Task dynamics of an example ZI neuron (**e**) and DA neuron (**f**). Action potentials in single trials are shown by rasters, and average activity is shown by spike density functions aligned on each key trial event (left) and on unpredicted intertrial events (right). Left: activity in NP (upper, red) versus FP trials (upper, blue) and novel trials (bottom, red) versus familiar trials (bottom, blue). Trials are shown separately for contralateral and ipsilateral target presentations (relative to the recording hemisphere). Trial outcome (reward)-related activity is shown combined for contralateral and ipsilateral trials. The ZI neuron (**e**, left) displayed novelty-presentation and novelty-prediction signals. Putative DA neuron (**f**, left) did not selectively respond to novelty-related events. **e,f** (right), in 1/6 of trials, unpredicted reward or no-reward cues occurred during intertrial intervals (ITIs). In contrast with the ZI neuron (**e**, right), the DA neuron (**f**, right) responded with phasic activation to unpredicted reward (but not to predicted reward; **f**, left), and it was suppressed by unpredicted no-reward cues (**f**, right). This combined pattern indicated that it signaled reward-prediction errors, but not novelty-prediction errors.

neuron preferentially increased its activity in anticipation of gaze shifts to obtain novel objects in NP trials, and in response to novel objects themselves (Fig. 1e, red trace). Also, this neuron encoded information about the monkey's upcoming novelty-seeking actions: (1) its responses were spatial, being increased during trials in which the peripheral object was presented on the contralateral versus ipsilateral hemifield (relative to the recording site), (2) its responses were higher when its activity was aligned to the time of the fractal acquisition versus object onset, and (3) it ramped up its activity in anticipation of the monkey obtaining the opportunity to gaze at the novel object. As well as signaling novelty predictions, this neuron also signaled spatial and motor information that is ideally suited to regulate novelty-seeking gaze shifts at visual objects.

Single DA neuron signals reward-prediction errors but not novelty predictions. We next asked whether value coding DA neurons

signal novelty predictions. We recorded the discharge activity of putative DA neurons from SNC^{8,9,45}. To help to identify DA neurons with reward value-related activity, we augmented a small fraction of ITIs to include two types of stimulus that have been extensively used for this purpose in previous studies^{8,9,45–48}: unpredicted rewards, and no-reward cues indicating reward omission (Fig. 1e, right). On the basis of previous findings, we expect a canonical value-coding DA neuron to signal positive reward-prediction errors following unpredicted rewards, including (1) excitation to unexpected rewards, (2) relative insensitivity to predicted rewards and (3) inhibition to the unexpected no-reward cue.

If a neuron that is sensitive to reward prediction is also sensitive to novelty-related predictions, it should respond to unpredicted presentations of novel objects (during novelty-inspecting trials), and to unpredicted presentations of objects that predict the opportunity to gaze at novel objects during novelty-seeking trials (NP trials).



An example of a putative DA neuron is shown in Fig. 1f. This neuron showed the canonical response pattern to reward-related stimuli: excitation by unpredicted rewards during the ITI, no response to fully predicted rewards during the task and inhibition by unpredicted no-reward cues during the ITI. However, this neuron did not display differential activation in response to NP versus FP objects, nor was it modulated by the relatively unexpected presentation of novel objects in novelty-inspecting trials. Thus, this neuron was relatively insensitive to object novelty or novelty-prediction errors.

Also, this putative DA neuron did not respond to the NP, FP, F and N objects even though they were associated with the 100% chance of getting a reward, mirroring many previous studies in primates that studied DA in tasks with fixed rewards and trial timing⁴⁹. Because DA neurons are highly sensitive to the subject's uncertainty and beliefs about reward and its timing^{50,51}, it is possible that this lack of cue response is related to the capacity and accuracy of time-keeping in primates versus, for example, rodents; but this should be explored in future studies.

Population responses of the ZI and the dopaminergic pathway.

We found that population-level responses were very similar to the single-neuron results in Fig. 1. There was a prominent population of ZI neurons that was preferentially excited in contralateral novelty-seeking and novelty-inspecting trials during the initial object presentation (Fig. 2a,b and Supplementary Fig. 4c). Like the example ZI neuron in Fig. 1e, average activity of task-sensitive ZI neurons predicted contralateral gaze shifts to NP objects and responded to the novel objects themselves in novelty-inspecting trials (Fig. 2a and Supplementary Fig. 4). The magnitude of these novelty anticipation signals in novelty-seeking trials and novelty presentation-related signals in novelty-inspecting trials were correlated across ZI neurons (Supplementary Fig. 4c), suggesting that these signals are part of coherent novelty-seeking processes.

Compared to the ZI, most DA neurons displayed stronger responses to unexpected reward versus no-reward cues (Fig. 2c,d and Supplementary Figs. 5,6), but the same neurons did not show average selective activity related to novelty prediction or inspection (Fig. 2a,b). As a population, DA neurons did not show preferential

responses to NP stimuli or novel stimuli themselves during the initial peripheral presentation or during free viewing (Fig. 2a and Supplementary Figs. 5,6).

We also recorded neuronal responses in the Lhb, which exert strong inhibitory control over DA value coding neurons⁵² and whose responses to reward value are opposite to those of DA neurons^{52–56}. As expected, the majority of Lhb neurons were strongly activated by unexpected no-reward cues and were inhibited by unexpected reward delivery (Fig. 2c,d and Supplementary Fig. 7). Like DA neurons, Lhb neurons were on average not strongly modulated by novelty (Fig. 2a,b). Additional neuron-by-neuron analyses revealed no relationship between novelty-related and reward-related signals in ZI, DA, or Lhb populations (Supplementary Figs. 4,5 and 7). So, the dissociation between reward-related and novelty-related processing extends beyond DA neurons, to an upstream area, the Lhb, which plays a central role in motivational and value-learning circuitry.

The locations of all neurons analyzed in Fig. 2 are shown in Fig. 2e. Novelty-related signals were most often found in the ZI, particularly in the caudal lateral ZI, above the posterior tail of the subthalamic nucleus (Supplementary Fig. 3b,c), whereas reward value-prediction error signals were most often found in the SN and Lhb.

Our results thus far show that population ZI activity reflects predictions about novel objects and the actions needed to obtain them (Supplementary Fig. 8), and that the Lhb and value-coding DA neurons are relatively insensitive to novelty. These results held true during novelty-familiarity learning (Supplementary Fig. 9), suggesting that they were not specific to the task conditions in Fig. 1a.

The lack of novelty sensitivity in the Lhb–DA pathway raises the question: which other brain areas predict or respond to novelty in our task? The basal forebrain (BF) contains a functional group of neurons that is sensitive to both unexpected deliveries of reward and the presentation of novel objects⁴⁷. We therefore tested whether these BF neurons responded to novelty in our task and carried signals necessary for motivating novelty seeking, a prediction of novelty in NP trials. Following the presentation of novel objects, BF neurons displayed a rapid phasic activation (Supplementary Fig. 10a,b), replicating our previous work⁴⁵, but they did not signal

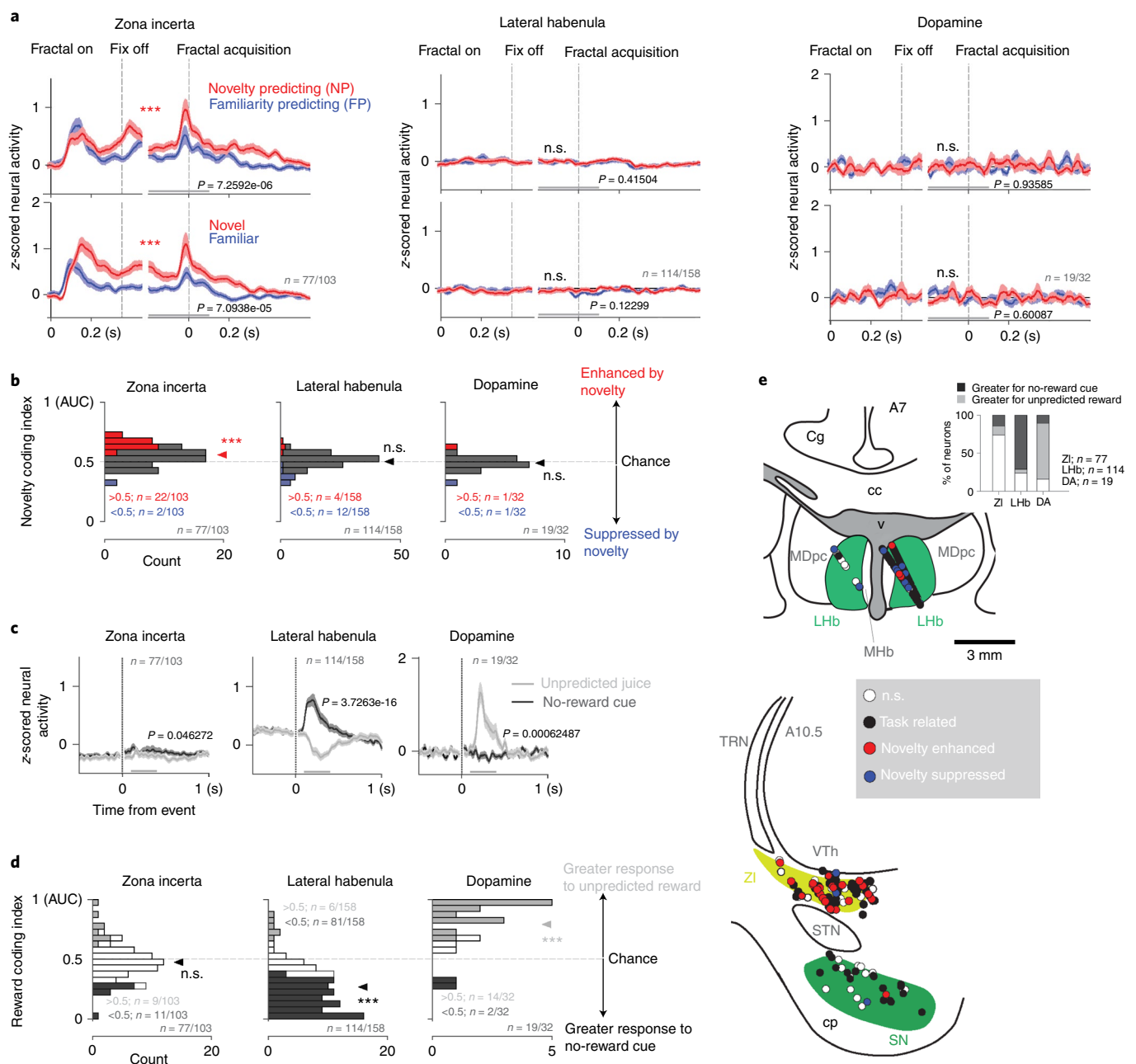
Fig. 2 | Novelty-seeking signals in the ZI. **a**, Average activity of all recorded neurons that displayed event-related variance in the ZI, habenula, and DA populations. Because ZI activity was spatially selective, contralateral trials are shown here (also see Supplementary Figs. 4,5,7). NP (upper, red) versus FP trials (upper, blue) and novel (bottom, red) versus familiar trials (bottom, blue). Error bars denote s.e.m.. Gray lines in each activity plot indicate windows in which statistical tests were performed across average activity. *P* values are indicated. Asterisks indicate a significant difference between responses in NP and FP trials, or novel and familiar trials ($***P < 0.001$, Wilcoxon signed-rank test); n.s. $P > 0.05$. **b**, Histograms of single neurons' novelty coding indices are shown for each area. To summarize novelty sensitivity, discrimination indices (area under the receiver operating characteristic curve (AUC)) compared all novelty-related trials (NP and novel) versus all familiar-related trials (FP and familiar) during the window in which habenula–DA neurons are known to respond to reward predictions (50 ms from object onset to the 'go-cue'). Red and blue bars indicate neurons with significantly larger (red) and smaller (blue) activations during novel versus familiar trials ($P < 0.05$, Wilcoxon rank-sum test). Arrowheads indicate mean of the distributions. Asterisks indicate significant difference from (0.5) chance ($***P < 0.001$, Wilcoxon signed-rank test); n.s. $P > 0.05$. Only the ZI (left) displayed a significant average novelty sensitivity (ZI, $P = 1.2 \times 10^{-6}$; habenula, $P = 0.36$; DA, $P = 0.33$). **c**, Averaged ITI unpredicted event activity of all neurons in **a**. Error bars denote s.e.m. *P* values comparing activity during ITI events are shown (Wilcoxon signed-rank test). Thick gray lines below denote analyses windows. **d**, The ZI (left) contained relatively small numbers of unpredicted reward-enhanced and unpredicted no-reward cue-enhanced neurons; by contrast, the habenula (middle) had more neurons that were more suppressed by reward ($P < 0.01$, $P = 1.0 \times 10^{-15}$) and DA (right) had more neurons that were relatively more enhanced by reward ($P < 0.01$, $P = 5.6 \times 10^{-15}$). Habenula and DA average discrimination (arrowhead) of reward versus no-reward events were highly significant ($***P < 0.001$, habenula, $P = 4.8 \times 10^{-16}$, DA, $P = 7.2 \times 10^{-4}$, Wilcoxon signed-rank test), but in opposite directions. Across all three areas, reward and novelty discrimination indices were uncorrelated (Supplementary Figs. 4,5,7). Indices in **d**: discrimination between unpredicted reward and unpredicted no-reward events (AUCs). Reward enhanced: gray; reward suppressed: black ($P < 0.05$, Wilcoxon rank-sum test). **e**, Reconstruction of recording sites. Circles indicate recorded neurons. Black filled circles: neurons with significant task-related modulation. Red and blue circles: neurons showing significant novelty-enhanced and -suppressed responses, respectively (same neurons as in **b**). White circles: neurons with no significant task-related variance. Habenula neurons (recorded from A6 to A7) are shown in the upper coronal plane (A7). ZI and DA neurons (recorded from A9 to A12) are shown on the bottom coronal plane (A10.5). Upper inset indicates the proportion of neurons showing relative excitation (gray), inhibition (black), or no modulation (white) in response to unpredicted reward versus unpredicted no-reward cues. Cg, cingulate cortex; MDpc, medial dorsal thalamic nucleus, parvocellular division; MHb, medial habenula; TRN, thalamic reticular nucleus; VTh, ventral thalamus; STN, subthalamic nucleus; cc, corpus callosum; v, ventricle; cp, cerebral peduncle.

novelty predictions in novelty-seeking trials. Thus, BF neurons respond to novel object presentations, but are unlikely to drive novelty seeking online (that is, on the short time-scale of a single trial or a gaze shift).

Causal manipulations link ZI neural activity and novelty seeking. We have shown that ZI neurons encode information that is necessary and sufficient to mediate novelty-seeking gaze shifts. We next hypothesized that temporary disruptions of ZI circuitry would impair novelty-seeking bias. To test this, we injected the GABA_A agonist muscimol into the regions of ZI that were enriched with novelty-seeking-related neurons (Fig. 2). We compared novelty bias (Fig. 1c) before and during ZI inactivation (monkey S, $n=6$; monkey R, $n=5$) and found that it was reduced after inactivation (Fig. 3a,b and Supplementary Fig. 11). In particular, the novelty bias was significantly reduced by the inactivation during trials in which gaze shifts were made to the contralateral visual

hemifield (relative to the injection site; Supplementary Fig. 11), but not during intermixed ipsilateral trials. This result provides an internal control⁵⁷ suggesting that the inactivation-induced effects were not simply due to general changes in motivation or engagement, and it is in line with the strong contralateral spatial selectivity in ZI neural activity (Fig. 1e and Supplementary Fig. 4b). Also, during inactivation sessions, the novelty bias was mostly quenched (Fig. 3b, y -axis; Supplementary Fig. 11), but not during sham sessions (4 in monkey R and 13 in monkey S; Supplementary Fig. 11).

How does the ZI implement its influence on novelty-seeking actions? The ZI has a strong reciprocal connection with the superior colliculus—a key region that regulates saccadic eye movements and spatial attention³⁷. To test whether the ZI regions involved in novelty seeking have strong access to saccadic circuitry, we performed low-intensity electrical stimulation within ZI regions that are enriched with novelty-excited neurons. Stimulation was initiated at



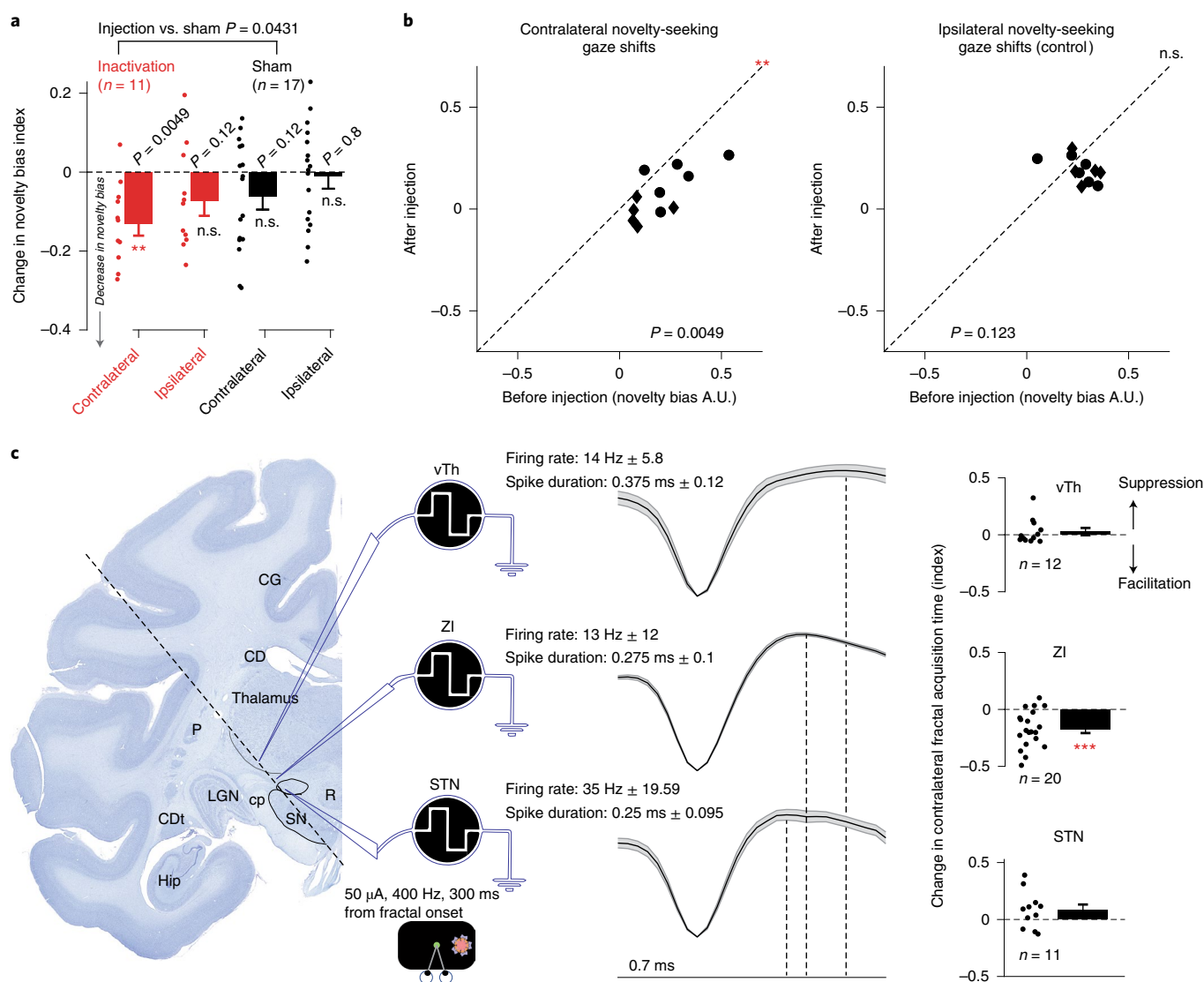


Fig. 3 | ZI is causally related to novelty seeking. **a, b**, Temporary pharmacological inactivation of ZI regions enriched with novelty-related neurons disrupts novelty seeking. **a**, Change in novelty-seeking bias (Fig. 1c) after versus before ZI inactivation. ZI inactivation most strongly reduces novelty-seeking bias during trials in which gaze shifts were contralateral to the site of the injection, matching the spatial selectivity of ZI (left red bar). Data from sham sessions ($n = 17$; two right bars) are shown for contralateral and ipsilateral trials. $**P < 0.01$, Wilcoxon signed-rank test. Above the bars is the result comparing the average of the contralateral and ipsilateral trials during inactivation sessions versus sham sessions ($P = 0.0431$, Wilcoxon rank-sum test). Single session changes are shown as dots next to the bars. Z-scored response times shown in Supplementary Fig. 11 indicate that novelty seeking was particularly reduced during inactivation. **b**, Single-session data are shown for contralateral (left) and ipsilateral (right) trials. P values comparing before and during inactivation data are indicated. Diamonds, monkey R; circles, monkey S. **c**, Low-intensity electrical stimulation of ZI regions enriched with novelty-related neurons but not stimulation of neighboring brain areas facilitates contralateral target object acquisition gaze behavior. Left, example recording and electrical stimulation path (dotted line) shown on a Nissl stain coronal section through the ZI. Middle electrophysiological markers of each brain region. Average firing rates, action potential wave form shapes (\pm s.e.m.; entire length of wave corresponds to 0.7 ms), and action potential wave form durations (dotted lines) are shown. Right, electrical stimulation of ZI (middle), but not of the vTh above ZI or the STN below ZI, facilitates saccadic target acquisition ($***P < 0.001$, Wilcoxon signed-rank test; STN and vTh, $P > 0.05$). Single sessions are shown as dots around the mean (bar). Error bar represents s.e.m. across sessions. The change in latency of gaze shifts (index) is calculated as the difference between stimulation trials and no-stimulation trials divided by their sum. CD caudate; CDt caudate tail; Hip hippocampus; LGN lateral geniculate nucleus; P putamen, R red nucleus; other anatomical regions are as defined in Fig. 2.

object onset while the monkeys continued to fixate the central spot (Fig. 1a) and ended 50 ms before the go-cue (Fig. 3c). ZI stimulation facilitated upcoming contralateral object acquisition gaze shifts (Fig. 3c, right-middle), but not ipsilateral ones (Wilcoxon signed-rank test; $P > 0.05$). This was again consistent with the contralateral spatial preference in ZI neural activity and with the spatially specific effects of inactivation experiments (Fig. 3a,b). By contrast, stimulation

of nearby regions did not facilitate saccades (Fig. 3c). Additional anatomical examination confirmed that the region of ZI that is enriched with neurons that mediate novelty seeking is connected to the brainstem, including the SC (Supplementary Fig. 17).

Together, the pharmacological and electrical stimulation experiments indicate that the ZI directly contributes to novelty seeking and can regulate primate gaze.

High channel neural recording identifies the temporal cortex as a potential key source of novelty predictions. Next, we sought to identify the neural sources of the novelty predictions that the ZI uses to anticipate and promote novelty-seeking behavior. The findings in Fig. 2 indicate that the habenula–DA pathway is not the source of novelty predictions in the ZI.

Instead, we hypothesized that frontal and temporal cortical regions that prominently project to the ZI may provide novelty predictions to the ZI. We recorded thousands of neurons in 17 different brain regions including the temporal cortex, amygdala, hippocampus and prefrontal cortices (Fig. 4a). During these neural recordings, monkeys S and L participated in the novelty-seeking/inspecting task (Fig. 1a).

We screened for brain regions that contained neurons that displayed the pattern of activity we observed in the ZI: selective prediction of the opportunity to gaze at novel objects (that is, novelty prediction) and selective response to the initial presentation of novel objects themselves (Figs. 1e and 2a). This revealed that the AVMTC was enriched with such novelty-seeking-related neurons (Fig. 4a). Similar results were obtained from analyses of multi-unit signals (Supplementary Fig. 12), and within each animal (Supplementary Fig. 13).

The AVMTC includes the anterior medial inferotemporal cortex and the perirhinal cortex, spanning from approximately 3 mm posterior to the anterior commissure to the temporal pole⁵⁸. This region of the primate brain responds to presentations of novel objects (Supplementary Fig. 14) and participates in object memory^{38,39,58–60}. Crucially, the AVMTC displayed a key novelty-prediction signal (Fig. 4a–c and Supplementary Fig. 14). So like the ZI, AVMTC neurons signal the novelty of incoming sensory information and actively predict the opportunity to gaze at novel objects (Fig. 4b, c and Supplementary Figs. 15,16). And importantly, the magnitude of AVMTC neurons' novelty-prediction responses in NP

trials correlated with the magnitude of the neurons' responses to the presentation of novel objects, suggesting that the two neural responses may reflect a single process of novelty seeking (Fig. 4b and Supplementary Fig. 15).

As in rodents^{61–63}, injecting anterograde and retrograde tracers into the AVMTC produced labeling in the ZI, supporting the notion that the AVMTC and the ZI are a part of an anatomical network for novelty seeking (Fig. 4d and Supplementary Figs. 17,18) that has strong access to brainstem oculomotor circuitry via the ZI.

To further study the organization of this network, we next tested whether novelty-related signals can be detected in the AVMTC earlier than in the ZI. We analyzed the latency of novelty-related signals in the activity of single neurons during novel versus familiar trials in which novel objects appeared at fractal onset, and the latency of novelty predictions during NP versus FP trials (Methods). Novelty presentation responses (sometimes referred to as 'novelty detection' signals) (Fig. 4e, left) and novelty-prediction signals (Fig. 4e, right and Supplementary Fig. 16b) occurred earlier in the AVMTC than the ZI, suggesting that the AVMTC could be a source of novelty-related information in ZI neurons.

So, do AVMTC novelty predictions already contain the necessary information to guide novelty-seeking actions, or do they undergo sensorimotor transformations to acquire the key action-related variables present in ZI activity (such as information about locations of objects and the timing of upcoming novelty-seeking gaze shifts; Fig. 2 and Supplementary Fig. 4)? Our analyses support the latter possibility.

First, AVMTC neurons had strong activity driven by object presentation, and ZI neurons most strongly increased their activity in anticipation of novelty-seeking gaze shifts (compare Fig. 4c with Fig. 2a). We quantified this trend on a neuron-by-neuron basis. To do this, we calculated whether activity was more strongly driven by object presentation or by object acquisition gaze shifts (Fig. 4f,

Fig. 4 | The AVMTC is a prominent cortical source of novelty-prediction signals. **a**, High channel count semi-chronic array recordings revealed that the AVMTC is highly enriched in neurons that displayed novelty-seeking control signals observed in ZI (Fig. 2). Neurons that displayed task event sensitivity (Kruskal–Wallis test; Methods) and discriminated novelty predictions (NP versus FP) and novelty presentations (novel versus familiar) with the same sign are defined as novelty-seeking neurons because they display the key signals theoretically required to drive novelty seeking. A neuron was defined as novelty-seeking related if it passed this criterion during either contralateral or ipsilateral trials, so the results were not biased to find spatially selective (or unselective) regions. The percentage of novelty-seeking neurons is shown for 17 brain areas. The two numbers by each bar indicate the number of novelty-seeking neurons and the total recorded neurons. The AVMTC has a higher ratio of novelty-seeking neurons than each of the other areas (red bar; $P < 0.05$; tested by 1,000 permutations, Bonferroni corrected). **a**, Small inset on left: model of semi-chronic high channel-count array with 124 independently movable electrodes on monkey's skull. **a**, Large inset on right bottom: model of recording array superimposed on a sagittal magnetic resonance imaging (MRI) slice of the brain. Electrodes from a computed tomography (CT) scan are also shown. Locations of AVMTC novelty-seeking-related neurons across all recording sessions in this monkey (S) are represented by red dots. **a**, Small inset on right, bottom: electrolytic marking lesion in AVMTC of monkey L at a location of a NP neuron. **b**, In both AVMTC and ZI, the magnitude of novelty prediction during the novelty-seeking trials was correlated with the magnitude of novelty responses in novelty-inspecting trials. Hence, novelty-'detection' responses (in novelty-inspecting trials) and novelty-prediction responses (in novelty-seeking trials) are linked. AUC values from ROC analyses are set up such that values greater than 0.5 indicate higher discharge rates on trials with novelty predictions (y-axis) or novel object presentations (x-axis). Each dot represents a neuron. Red and magenta dots indicate neurons displaying significant novelty-prediction and novelty-presentation responses, respectively (Wilcoxon rank-sum test; $P < 0.05$). Cyan dots indicate neurons showing both. Black dots indicate other neurons with significant task-related modulation (Kruskal–Wallis test; $P < 0.05$) but no novelty-related modulation. White dots indicate neurons with no significant task event modulation. Gray lines indicate least squares fits. Spearman's correlation results are reported by each scatter plot. **c**, Average activity of AVMTC novelty-seeking neurons (preselected in contralateral trials by analyses of activity during the fractal acquisition epoch) shown here in ipsilateral trials. Conventions and statistical tests are the same as Fig. 2. Shaded region is s.e.m. Here, neurons ($n = 44$) that displayed task event variance (Kruskal–Wallis test; Methods) and discriminated NP versus FP trials and novel versus familiar trials with the same sign (either with novelty-related excitation or inhibition) are included ($P < 0.05$, Wilcoxon rank-sum test). ***In top and bottom plots denotes $P < 7.7 \times 10^{-9}$ (Wilcoxon signed-rank test). **d**, Anterograde tracer injections into the AVMTC produce labeled axons in the ZI. **e**, left, Cumulative distributions of single neurons' latencies of novelty signals in NP trials; right, novelty predictions in NP trials. Left plot: ZI $n = 58$; AVMTC $n = 366$; $P = 0.0002$; right plot: ZI $n = 48$; AVMTC $n = 289$; $P = 0.008$ (Wilcoxon rank-sum test). **f**, AVMTC neurons are relatively more related to the onset of visual stimuli, while ZI neurons are relatively more related to gaze motor behavior. **f**, Left, to quantify whether a neuron's response has spatial sensitivity we computed a spatial index as the discrimination (AUC) comparing contralateral trials with ipsilateral trials during 200 ms before to 100 ms after fractal object acquisition. **f**, Right, ZI neurons have relatively more motor information than the AVMTC to control action. To quantify whether a neuron's response is relatively more visual or motor related we computed a motor index as the discrimination comparing responses aligned on object presentation (time window: 50 ms from object onset to the 'go-cue') versus aligned on object acquisition (time window: 200 ms before to 100 ms after object acquisition) in contralateral NP trials. In **f** all task-related neurons are included (ZI $n = 77$; AVMTC $n = 465$). *** $P < 0.001$, ** $P < 0.01$, * $P < 0.05$, Wilcoxon rank-sum tests.

right) using an approach traditionally applied to assess a neuron's or a brain region's relative position along the sensorimotor continuum^{64,65}. We found that the AVMTC was indeed more 'visual' than the ZI, displaying relatively stronger activation during object presentation than object acquisition ($P = 8.2 \times 10^{-7}$; Wilcoxon rank-sum test). By contrast, the ZI was more driven by the object acquisition gaze shifts than the AVMTC (Fig. 4f, right). Second, to assess which brain area contained more information about novelty-seeking gaze behavior, we measured single neurons' encoding of the spatial locations of peripheral fractal objects (Fig. 4f, left). This revealed that AVMTC neurons were spatially selective, but much less so than ZI neurons (Fig. 4f, left). The directions of upcoming gaze shifts were more strongly encoded in ZI activity ($P = 4.1 \times 10^{-14}$; Wilcoxon rank-sum test). Third, in the AVMTC the magnitude of neurons' novelty-prediction responses in NP trials correlated with the magnitude of the same neurons' activity in response to the presentation

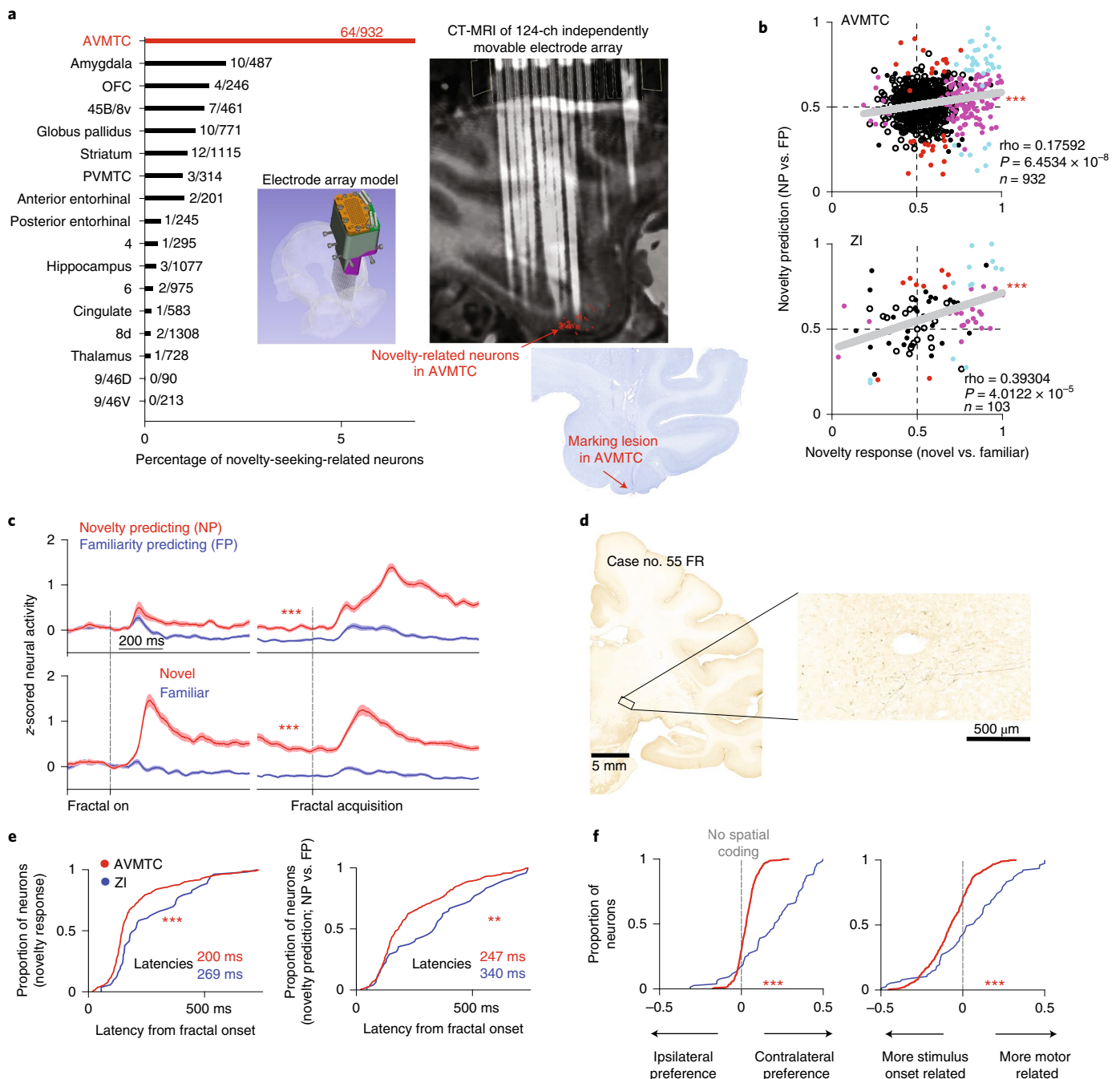
of novel objects during both contralateral and ipsilateral trials, whereas in the ZI this was only the case during contralateral trials (Supplementary Fig. 15).

In sum, these results show that AVMTC activity reflects predictions of novel objects and that this relatively earlier signal in the AVMTC contains less spatial and motor-control information than in the ZI.

Discussion

Anticipation of future novel objects is a key feature of primate intelligence, expressed in our gaze, and is a component of our innate curiosity¹. But it has remained unknown whether there is a brain area that anticipates novel visual objects and causally contributes to seeking them before they are present.

We show that monkeys prefer novelty, as reflected in their behavioral seeking of the novelty 'for its own sake' (Fig. 1c,d); that neu-



rons in the primate ZI, particularly above the posterior end of the subthalamic nucleus in the caudal lateral ZI, predict future novelty; that this neural signal increases before gaze shifts that will result in the presentation and subsequent experience of novel objects; and that inactivating these neurons disrupts novelty seeking. This control of novelty seeking by the ZI was independent of many DA and LHB neurons: many LHB and DA neurons had little response to novelty in a task in which novel objects had no extrinsic value. Finally, we identified the AVMTc as a potential source of novelty predictions. Overall, our data are consistent with a model in which the AVMTc identifies objects associated with future novelty, and the ZI transforms such novelty predictions to control gaze behavior, through interactions with the AVMTc and through its strong reciprocal connections with the superior colliculus and other regions in the brainstem (Supplementary Fig. 17).

Our results place the ZI in an important position in the circuitry that regulates motivated behavior in primates, and pave the way for future investigations of its other functions. The ZI receives input from higher-order cortical areas²⁹ and it is ideally positioned to transform sensory and cognitive information^{30,66,67}, transmitting it to subcortical regions rapidly to control motivation^{29,68}, action^{29,31,36} and attention^{30,31}. Future studies should obtain more information about how the distinct neuronal types^{28,29,31} and subregions^{36,69,70} of the ZI cooperate to enable its functions in novelty seeking and other behaviors. A recent paper has shown that GABAergic neurons in the rodent medial ZI are sensitive to states of arousal driven by the presence of novel objects and conspecifics and influence rodent approach behaviors to novel objects³⁵. These findings also highlight the need to investigate the primate ZI at a finer molecular level. Interestingly, the caudal lateral ZI, where many novelty-seeking neurons were found (Fig. 2 and Supplementary Fig. 3), could be anatomically distinct from other regions of the ZI owing to its sparse population of GABA neurons and presence of calbindin neurons⁷¹. But the functional significance of this observation, and of distinct ZI subregions in primates, remains unclear.

Our data expand the role of the AVMTc beyond processing of incoming novel objects and object memory formation, and are consistent with the idea that the AVMTc processes higher-order object information to control association and learning⁶⁰. Notably, our results show that the AVMTc not only associates objects with other 'known' objects, but also associates them with abstract information, such as with the prediction of future novelty. Thus, akin to how the reward system endows objects and actions with future rewards to regulate reward-seeking behaviors, the AVMTc could participate in the association of objects with future novelty to regulate novelty-seeking behavior.

We designed a task to study novelty seeking when novel objects have no primary extrinsic reward value. The purpose of our paper was not to discriminate among theories of DA at the level of reward-prediction errors (for example, learning versus online moment-by-moment control relative to rewards). Rather, we identified canonical reward-prediction error-coding DA neurons and LHB neurons using standard methods from macaque neurophysiology and tested their role in novelty seeking.

Our results do not indicate that the LHB–DA pathway is insensitive to novel objects when their novelty is a cue for a change in reward state, or in cases in which novelty provides an opportunity for new reward-associative learning. In fact, when new objects have reward values that monkeys have not yet learned, DA neurons do respond to novel objects and rapidly update their value representations as animals learn their object–reward associations^{18,46,72}. In mice, unexpected novel objects that are first perceived as threatening rapidly activate a specific DA population in the caudal-lateral SN that are involved in processing threatening and aversive events²⁴. When mice are presented with neutral novel odors, responses of DA neu-

rons are highly variable across odors and animals, in a manner that is roughly correlated with preferences for the odors⁷³. Another study found no novelty-related selectivity in medial DA neurons, but did observe signals related to the subjective value of social behavior²³. These studies show that DA neurons could become activated by novel stimuli when animals perceive them as valuable or important for guiding reward or punishment-related behaviors^{18,24,72,74}. The data in our study indicate that reward-prediction error-coding DA neurons are mostly insensitive to novelty when animals are strongly motivated to seek novelty for its own sake rather than as a tool to obtain extrinsic rewards.

DA neurons are located in multiple regions, including the ventral tegmental area (VTA) and SNc, and have distinct input and output projections⁷⁵. We concentrated on SNc because it is generally agreed on that spike shapes, firing rates and reward responses, in combination, are sufficient to identify SNc DA neurons in primates. As new methods become available, future studies will be able to assess DA signals of the VTA and of different subregions of the SNc in primates to understand whether our results generalize to other or all DA neuron populations.

Very little is known about the process that must precede the seeking of novel visual objects, that is, novelty detection and the algorithms that support it. Several computational theories provide various levels of formal description for why novelty signals that discriminate novel versus familiar objects could be present in many areas of the primate brain (Supplementary Fig. 14). Determining the algorithms of novelty detection in different brain areas, and the cell types that support them, may help us understand why apparently only a small number of brain areas signal novelty predictions necessary to control novelty seeking (Supplementary Fig. 14). Thus, discovering how neural networks detect novelty will be a crucial next step in understanding how the AVMTc–ZI pathway regulates the motivation to seek novel objects. Also, during gaze shifts many neural networks are recruited (Supplementary Fig. 19), and so how novelty detection and novelty-prediction signals in the AVMTc–ZI pathway regulate action through the SC (Supplementary Fig. 17) and other networks such as the basal ganglia will be another important direction for future work to reveal how predictions of novelty are transformed into action and mediate our innate curiosity.

Online content

Any methods, additional references, Nature Research reporting summaries, source data, extended data, supplementary information, acknowledgements, peer review information; details of author contributions and competing interests; and statements of data and code availability are available at <https://doi.org/10.1038/s41593-021-00950-1>.

Received: 20 April 2021; Accepted: 28 September 2021;
Published online: 13 December 2021

References

- Jaegle, A., Mehrpour, V. & Rust, N. Visual novelty, curiosity, and intrinsic reward in machine learning and the brain. *Curr. Opin. Neurobiol.* **58**, 167–174 (2019).
- Wang, T. & Mitchell, C. J. Attention and relative novelty in human perceptual learning. *J. Exp. Psychol. Anim. Behav. Process.* **37**, 436–445 (2011).
- Ghazizadeh, A., Griggs, W. & Hikosaka, O. Ecological origins of object salience: reward, uncertainty, aversiveness, and novelty. *Front. Neurosci.* **10**, 378 (2016).
- Loewenstein, G. The psychology of curiosity: a review and reinterpretation. *Psychological Bull.* **116**, 75 (1994).
- Butler, R. A. Discrimination learning by rhesus monkeys to visual-exploration motivation. *J. Comp. Physiological Psychol.* **46**, 95 (1953).
- Berlyne, D. E. Novelty and curiosity as determinants of exploratory behaviour. *Br. J. Psychol.* **41**, 68 (1950).

7. Cohen, J. Y., Haesler, S., Vong, L., Lowell, B. B. & Uchida, N. Neuron-type-specific signals for reward and punishment in the ventral tegmental area. *Nature* **482**, 85–88 (2012).
8. Schultz, W., Dayan, P. & Montague, P. R. A neural substrate of prediction and reward. *Science* **275**, 1593–1599 (1997).
9. Bromberg-Martin, E. S., Matsumoto, M. & Hikosaka, O. Dopamine in motivational control: rewarding, aversive, and alerting. *Neuron* **68**, 815–834 (2010).
10. Lisman, J. E. & Grace, A. A. The hippocampal–VTA loop: controlling the entry of information into long-term memory. *Neuron* **46**, 703–713 (2005).
11. Tapper, A. R. & Molas, S. Midbrain circuits of novelty processing. *Neurobiol. Learning Memory* **176**, 107323 (2020).
12. Duzsikiewicz, A. J., McNamara, C. G., Takeuchi, T. & Genzel, L. Novelty and dopaminergic modulation of memory persistence: a tale of two systems. *Trends Neurosci.* **42**, 102–114 (2019).
13. Kakade, S. & Dayan, P. Dopamine: generalization and bonuses. *Neural Netw.* **15**, 549–559 (2002).
14. Bunzeck, N. & Düzel, E. Absolute coding of stimulus novelty in the human substantia nigra/VTA. *Neuron* **51**, 369–379 (2006).
15. Wittmann, B. C., Bunzeck, N., Dolan, R. J. & Düzel, E. Anticipation of novelty recruits reward system and hippocampus while promoting recollection. *NeuroImage* **38**, 194–202 (2007).
16. Lak, A., Stauffer, W. R. & Schultz, W. Dopamine prediction error responses integrate subjective value from different reward dimensions. *Proc. Natl Acad. Sci. USA* **111**, 2343–2348 (2014).
17. Schultz, W. Updating dopamine reward signals. *Curr. Opin. Neurobiol.* **23**, 229–238 (2013).
18. Lak, A., Stauffer, W. R. & Schultz, W. Dopamine neurons learn relative chosen value from probabilistic rewards. *eLife* **5**, e18044 (2016).
19. Dabney, W. et al. A distributional code for value in dopamine-based reinforcement learning. *Nature* **577**, 671–675 (2020).
20. Bromberg-Martin, E. S. & Hikosaka, O. Midbrain dopamine neurons signal preference for advance information about upcoming rewards. *Neuron* **63**, 119–126 (2009).
21. McHenry, J. A. et al. Hormonal gain control of a medial preoptic area social reward circuit. *Nat. Neurosci.* **20**, 449–458 (2017).
22. Gunaydin, L. A. et al. Natural neural projection dynamics underlying social behavior. *Cell* **157**, 1535–1551 (2014).
23. Ranganath, C. & Rainer, G. Neural mechanisms for detecting and remembering novel events. *Nat. Rev. Neurosci.* **4**, 193–202 (2003).
24. Menegas, W., Babayan, B. M., Uchida, N. & Watabe-Uchida, M. Opposite initialization to novel cues in dopamine signaling in ventral and posterior striatum in mice. *eLife* **6**, e21886 (2017).
25. Huang, X. & Weng, J. Novelty and reinforcement learning in the value system of developmental robots. (2002).
26. Oudeyer, P.-Y., Kaplan, F. & Hafner, V. V. Intrinsic motivation systems for autonomous mental development. *IEEE Trans. Evolut. Comput.* **11**, 265–286 (2007).
27. Gottlieb, J., Lopes, M. & Oudeyer, P.-Y. in *Recent Developments in Neuroscience Research on Human Motivation* 149–172 (Emerald, 2016).
28. Lin, C. S., Nicolelis, M. A., Schneider, J. S. & Chapin, J. K. Jr. GABAergic pathway from zona incerta to neocortex: clarification. *Science* **251**, 1162 (1991).
29. Lin, C. S., Nicolelis, M. A., Schneider, J. S. & Chapin, J. K. A major direct GABAergic pathway from zona incerta to neocortex. *Science* **248**, 1553–1556 (1990).
30. Mitrofanis, J. Some certainty for the “zone of uncertainty”? Exploring the function of the zona incerta. *Neuroscience* **130**, 1–15 (2005).
31. Wang, X., Chou, X.-I., Zhang, L. I. & Tao, H. W. Zona incerta: an integrative node for global behavioral modulation. *Trends Neurosci.* **43**, 82–87 (2020).
32. Zhao, Z.-d et al. Zona incerta GABAergic neurons integrate prey-related sensory signals and induce an appetitive drive to promote hunting. *Nat. Neurosci.* **22**, 921–932 (2019).
33. Tonelli, L. & Chiaraviglio, E. Enhancement of water intake in rats after lidocaine injection in the zona incerta. *Brain Res. Bull.* **31**, 1–5 (1993).
34. Chometton, S. et al. The rostromedial zona incerta is involved in attentional processes while adjacent LHA responds to arousal: c-Fos and anatomical evidence. *Brain Struct. Funct.* **222**, 2507–2525 (2017).
35. Ahmadlou, M. et al. A cell type-specific cortico-subcortical brain circuit for investigatory and novelty-seeking behavior. *Science* **372**, 6543 (2021).
36. May, P. J. & Basso, M. A. Connections between the zona incerta and superior colliculus in the monkey and squirrel. *Brain Struct. Funct.* **223**, 371–390 (2018).
37. Krauzlis, R. J., Lovejoy, L. P. & Zénon, A. Superior colliculus and visual spatial attention. *Annu. Rev. Neurosci.* **36**, <https://doi.org/10.1146/annurev-neuro-062012-170249> (2013).
38. Brown, M. W. & Aggleton, J. P. Recognition memory: what are the roles of the perirhinal cortex and hippocampus? *Nat. Rev. Neurosci.* **2**, 51–61 (2001).
39. Murray, E. A. & Richmond, B. J. Role of perirhinal cortex in object perception, memory, and associations. *Curr. Opin. Neurobiol.* **11**, 188–193 (2001).
40. Lauwereyns, J., Watanabe, K., Coe, B. & Hikosaka, O. A neural correlate of response bias in monkey caudate nucleus. *Nature* **418**, 413–417 (2002).
41. Kim, H. F., Ghazizadeh, A. & Hikosaka, O. Separate groups of dopamine neurons innervate caudate head and tail encoding flexible and stable value memories. *Front. Neuroanat.* **8**, 120 (2014).
42. Jutras, M. J. & Buffalo, E. A. Recognition memory signals in the macaque hippocampus. *Proc. Natl Acad. Sci. USA* **107**, 401–406 (2010).
43. Zhang, K., Chen, C. D. & Monosov, I. E. Novelty, salience, and surprise timing are signaled by neurons in the basal forebrain. *Curr. Biol.* **29**, 134–142. e133 (2019).
44. Tachibana, Y. & Hikosaka, O. The primate ventral pallidum encodes expected reward value and regulates motor action. *Neuron* **76**, 826–837 (2012).
45. Matsumoto, M. & Hikosaka, O. Two types of dopamine neuron distinctly convey positive and negative motivational signals. *Nature* **459**, 837–841 (2009).
46. Hollerman, J. R. & Schultz, W. Dopamine neurons report an error in the temporal prediction of reward during learning. *Nat. Neurosci.* **1**, 304–309 (1998).
47. Joshua, M., Adler, A., Mitelman, R., Vaadia, E. & Bergman, H. Midbrain dopaminergic neurons and striatal cholinergic interneurons encode the difference between reward and aversive events at different epochs of probabilistic classical conditioning trials. *J. Neurosci.* **28**, 11673–11684 (2008).
48. Eshel, N. et al. Arithmetic and local circuitry underlying dopamine prediction errors. *Nature* **525**, 243–246 (2015).
49. Nakahara, H., Itoh, H., Kawagoe, R., Takikawa, Y. & Hikosaka, O. Dopamine neurons can represent context-dependent prediction error. *Neuron* **41**, 269–280 (2004).
50. Babayan, B. M., Uchida, N. & Gershman, S. J. Belief state representation in the dopamine system. *Nat. Commun.* **9**, 1891 (2018).
51. Fiorillo, C. D., Newsome, W. T. & Schultz, W. The temporal precision of reward prediction in dopamine neurons. *Nat. Neurosci.* **11**, 966–973 (2008).
52. Matsumoto, M. & Hikosaka, O. Lateral habenula as a source of negative reward signals in dopamine neurons. *Nature* **447**, 1111–1115 (2007).
53. Matsumoto, M. & Hikosaka, O. Negative motivational control of saccadic eye movement by the lateral habenula. *Prog. Brain Res.* **171**, 399–402 (2008).
54. Matsumoto, M. & Hikosaka, O. Representation of negative motivational value in the primate lateral habenula. *Nat. Neurosci.* **12**, 77–84 (2009).
55. Salas, R., Baldwin, P., De Biasi, M. & Montague, R. BOLD responses to negative reward prediction errors in human habenula. *Front. Hum. Neurosci.* **4**, 36 (2010).
56. Bromberg-Martin, E. S. & Hikosaka, O. Lateral habenula neurons signal errors in the prediction of reward information. *Nat. Neurosci.* **14**, 1209–1216 (2011).
57. White, J. K. et al. A neural network for information seeking. *Nat. Commun.* **10**, 5168 (2019).
58. Xiang, J.-Z. & Brown, M. Differential neuronal encoding of novelty, familiarity and recency in regions of the anterior temporal lobe. *Neuropharmacology* **37**, 657–676 (1998).
59. Haskins, A. L., Yonelinas, A. P., Quamme, J. R. & Ranganath, C. Perirhinal cortex supports encoding and familiarity-based recognition of novel associations. *Neuron* **59**, 554–560 (2008).
60. Tamura, K. et al. Conversion of object identity to object-general semantic value in the primate temporal cortex. *Science* **357**, 687–692 (2017).
61. Furtak, S. C., Wei, S. M., Agster, K. L. & Burwell, R. D. Functional neuroanatomy of the parahippocampal region in the rat: the perirhinal and postrhinal cortices. *Hippocampus* **17**, 709–722 (2007).
62. Tomás Pereira, I., Agster, K. L. & Burwell, R. D. Subcortical connections of the perirhinal, postrhinal, and entorhinal cortices of the rat. I. Afferents. *Hippocampus* **26**, 1189–1212 (2016).
63. Agster, K. L., Tomás Pereira, I., Saddoris, M. P. & Burwell, R. D. Subcortical connections of the perirhinal, postrhinal, and entorhinal cortices of the rat. II. Efferents. *Hippocampus* **26**, 1213–1230 (2016).
64. Sommer, M. A. & Wurtz, R. H. Composition and topographic organization of signals sent from the frontal eye field to the superior colliculus. *J. Neurophysiol.* **83**, 1979–2001 (2000).
65. Schall, J. D. The neural selection and control of saccades by the frontal eye field. *Philos. Trans. R. Soc. Lond. B* **357**, 1073–1082 (2002).
66. Trageser, J. C. et al. State-dependent gating of sensory inputs by zona incerta. *J. Neurophysiol.* **96**, 1456–1463 (2006).
67. Barthó, P. et al. Cortical control of zona incerta. *J. Neurosci.* **27**, 1670–1681 (2007).
68. de Git, K. C. G. et al. Zona incerta neurons projecting to the ventral tegmental area promote action initiation towards feeding. *J. Physiol.* **599**, 709–724 (2021).
69. Ma, T. P. Saccade-related omnivectorial pause neurons in the primate zona incerta. *Neuroreport* **7**, 2713–2716 (1996).

70. Kita, T., Osten, P. & Kita, H. Rat subthalamic nucleus and zona incerta share extensively overlapped representations of cortical functional territories. *J. Comp. Neurol.* **522**, 4043–4056 (2014).
71. Watson, C., Lind, C. R. & Thomas, M. G. The anatomy of the caudal zona incerta in rodents and primates. *J. Anat.* **224**, 95–107 (2014).
72. Ljungberg, T., Apicella, P. & Schultz, W. Responses of monkey dopamine neurons during learning of behavioral reactions. *J. Neurophysiol.* **67**, 145–163 (1992).
73. Morrens, J., Aydin, Ç., van Rensburg, A. J., Rabell, J. E. & Haesler, S. Cue-evoked dopamine promotes conditioned responding during learning. *Neuron* **106**, 142–153.e147 (2020).
74. Costa, V. D., Tran, V. L., Turchi, J. & Averbeck, B. B. Dopamine modulates novelty seeking behavior during decision making. *Behav. Neurosci.* **128**, 556–566 (2014).
75. Watabe-Uchida, M., Zhu, L., Ogawa, S. K., Vamanrao, A. & Uchida, N. Whole-brain mapping of direct inputs to midbrain dopamine neurons. *Neuron* **74**, 858–873 (2012).

Publisher's note Springer Nature remains neutral with regard to jurisdictional claims in published maps and institutional affiliations.

© The Author(s), under exclusive licence to Springer Nature America, Inc. 2021

Methods

Statistics. All statistical tests are detailed in the Statistical Analyses section of Methods section and elsewhere when appropriate.

General procedures. Adult male rhesus monkeys (*Macaca mulatta*; aged 6–9 years old) were used for the electrophysiology experiments. All procedures conformed to the Guide for the Care and Use of Laboratory Animals and were approved by the Washington University Institutional Animal Care and Use Committee. A plastic head holder and plastic recording chamber were fixed to the skull under general anesthesia and sterile surgical conditions. For monkeys R, S and Z, large neuronal recording chambers were tilted and aimed at the SN, habenula and ZI. Their anterior-posterior extent included other regions of interest such as the BF. Monkey B's chambers were primarily aimed at the basal forebrain, ventral pallidum and the prefrontal cortex. After the monkeys recovered from surgery, they participated in the behavioral and neurophysiological experiments.

For acute recording experiments, recording sites were determined with a 1 mm spacing grid system and with the aid of magnetic resonance images (3T). This MRI-based estimation of neuron recording locations was aided by custom-built software (PyElectrode⁷⁰) and histology.

Single-unit recording was performed using glass-coated electrodes (Alpha Omega), epoxy-coated electrodes (FHC) and 16 and 32 channel linear arrays (v-probes, Plexon). In particular, for ZI and DA neurons, we used custom-modified epoxy electrodes with 1.2 to 2.5 M Ω impedance (FHC). Electrodes or linear arrays were inserted into the brain through a stainless steel guide tube and advanced by an oil-driven micromanipulator (MO-97A, Narishige). Signal acquisition (including amplification and filtering) was performed using a Plexon 40 kHz recording system. In these experiments, action potential waveforms were identified online by multiple time-amplitude windows, and the isolation was refined using offline clustering on the first three principal components and a measure of nonlinear energy (Plexon Offline Sorter).

In monkey S, we recorded 50 ZI neurons, one DA neuron and as control 11 thalamic neurons above the ZI. In monkey R, we recorded 53 ZI neurons, 78 habenula neurons, 20 DA neurons and as control 36 subthalamic neurons. In monkey Z, we recorded 80 habenula neurons, 11 DA neurons and as control eight basal forebrain neurons, seven subthalamic neurons and 14 thalamic neurons above the ZI. In monkey B, we recorded 15 basal forebrain neurons. The recordings (above) in monkey S were performed after the semi-chronic array was removed. During recording of each brain area, there were strong significant differences in single trial fractal object acquisition times between NP and FP trials ($P < 0.001$) and novel and familiar trials ($P < 0.001$; Wilcoxon rank-sum tests).

For monkeys L and S, we implanted semi-chronic high channel-count recording drives (LS124; Grey Matter). To aim the micro drives, we first acquired 3T magnetic resonance images of the monkeys' brains. We used these magnetic resonance images to aim the two micro drives towards the regions of interest, including the prefrontal cortex and the temporal cortex. We then attached MRI compatible chambers to the skull with MRI compatible ceramic screws (Thomas). After the animals recovered, we performed MRI with fiducials such that we could estimate and reconstruct the path of each electrode^{77,76–79}. Following this preoperative confirmation, we implanted both animals with 124-channel micro drives. These are detailed here: <https://www.graymatter-research.com/documentation-manuals>. Following craniotomy, we sealed the chamber and used a port to assess whether bacterial growth occurred. Following this safety precaution, we implanted the recording drives containing the electrodes and lowered all channels immediately beyond the dura. In this way, we minimized the impact of postoperative dura thickening on the electrode impedance and trajectory. Data from electrode channels were included in the study if: (1) postoperative CT images showed that the electrodes were in the brain and were following a trajectory that could be visualized; (2) if the electrode channel produced single units during the history of the array neuronal recordings; and (3) if the postoperative impedance was greater than 0.2 M Ω or single units were observed. This approach produced 108/124 channels in monkey L and 124/124 channels in monkey S. A key difference in success was due to the use of glass-coated electrodes (Alpha Omega) in monkey S versus thinner epoxy electrodes in monkey L (FHC). Recording locations of novelty-selective neurons were verified in several ways. First, we placed electrolytic marking lesions in monkey L^{80–82}. Second, for both animals, we acquired sequential CT images. These images were registered to the MRI and the locations of the electrodes were directly visualized. Third, as we moved we used functional and anatomical landmarks classically employed by our and other laboratories (e.g., electrophysiological patterns of brain areas such as the globus pallidus, striatum, anterior commissure, ventricles, lateral geniculate nucleus) to verify electrode locations further. Hence, for recording location estimation, we used histology, imaging and classic electrophysiological methods^{78,79,83}. The brain regions in the MRI were defined exactly as in previous studies^{78,79,83,84} with two exceptions. Posterior 45B and ventral 8 (8v) are hard to differentiate. We therefore grouped them together in this study (Supplementary Fig. 20). The AVMTc included the perirhinal cortex and medial TE (medial inferior temporal cortex) (Fig. 4a) and was defined widely along the anterior-posterior axis from approximately –3 mm relative to the anterior commissure, spanning to the temporal pole as in previous studies⁵⁸ (Supplementary Fig. 20 for anatomical

locations of array neural recording; also because of the complex shape of the striatum we included an additional three dimensional plot striatal neurons in Supplementary Fig. 21).

The semi-chronic drive contained electrodes with 1.5 mm spacing. Signal acquisition (including amplification and filtering) was performed using a Plexon 40 kHz recording system. Action potentials were identified in two manners. First, we used offline manual sorting (Plexon Offline Sorter). Second, we deployed a semi-supervised template matching based algorithm (Kilosort2) to sort the data and then corrected the results further to avoid oversplitting. To verify the key results of our approach, we also analyzed multi-unit activity (MUA), a bulk, average, unbiased measure. We defined MUA as signals that passed –2 s.d. but did not cross –3 s.d.

To identify the SN, we used standard landmarks such as the subthalamic nucleus, ZI and the thalamus. We identified putative DA neurons in the SN on the basis of classic electrophysiological criteria across monkey studies that have been replicated in optogenetically identified SN DA neurons^{89,45,75}: (1) a low background firing rate at around five spikes/s; (2) a wide spike waveform in clear contrast to neighboring neurons with a high background firing rate in the SN pars reticulata; and (3) a phasic excitatory activity caused by an unexpected reward delivery or trial start cue⁸⁵. Because medial DA populations in the VTA are harder to identify online by these criteria⁸⁶, we concentrated on the SN. We also recorded in the LHB, which is known to mirror medial motivational value coding DA neurons' activities reliably, including those in the VTA^{52,54}.

Histology. After the end of some recording sessions, we made electrolytic microlesions at the recording sites in monkey L (~20 μ A and 30 s). The monkey was deeply anesthetized using sodium pentobarbital and perfused with 10% formaldehyde. The brain was blocked and equilibrated with 10% sucrose. Frozen sections were cut every 50 μ m in the coronal plane. The sections were stained with cresyl-violet. Monkeys used for anatomical tracer injections were perfused in a similar way.

Tracer-related histology. Male macaque monkeys were used. Anatomical cases are from the collection of anatomical tracers from the laboratories of Dr. Price that have been digitized by the Monosov laboratory for further analyses. For those injections, Fluoro Ruby (case no. 55; 1 μ l @ 10%) and Lucifer Yellow (case no. 58; 0.5 μ l @ 10%) were used. For surgeries and MRI scan, anesthesia was induced by ketamine injection (10 mg/kg) and maintained with a gaseous mixture of oxygen, nitrous oxide and halothane. Animals were given analgesic (buprenorphine, 0.1 mg/kg, i.m.) postsurgery. Craniotomies were performed at the stereotaxic coordinates of the injection sites. Before the injections, recordings were performed along the trajectory of the injection site. This procedure helped refine the position of the injection site by controlling for the gray and white matter, sulci, and bottom of the brain; 1 μ l of Fluoro Ruby (FR; @ 10%) and 0.5 μ l of Lucifer Yellow (LY, @ 10%) were injected to the AVMTc of case no. 55 and case no. 58, respectively. Tracers were injected through micropipettes using air pressure. After each injection, the pipette was left in place for 30 min. After 14 days following the surgery, the animals were deeply anesthetized (ketamine, 10 mg/kg), overdosed with sodium pentobarbital (25–30 mg/kg) and perfused with phosphate-buffered saline followed by 4% paraformaldehyde solutions, first at pH 6.5, then at pH 9.5, and finally at pH 9.5 with 10% sucrose. The brain was removed and transferred through 10%, 20% and 30% sucrose solutions in phosphate buffer at 4°C. After this, brains were frozen in isopentane and dry ice and later cut into several series (12 and 10 series for case no. 55 and case no. 58, respectively) of coronal sections at 50 μ m thickness. Both FR and LY were processed immunohistochemically with an avidin-biotin-horseradish peroxidase technique using a Vectastain ABC kit^{87–90}. Additional cases 56 and 57 in Supplementary Materials were obtained from previously published FR cases (courtesy of Dr. Price) and were processed using the same methods as case 55.

Task. The behavioral task is displayed in Fig. 1a. The task began with the appearance of a small orange circular trial start cue at the center of the screen. The monkeys had to fixate this spot for 0.5 s. If the animal did not do this within 5 s, the trial aborted and the ITI started. Following successful fixation, a peripheral visual fractal object stimulus appeared 10 degrees visual angle from the fixation spot. The monkey had to continue to fixate the central fixation spot for 0.35 s or 0.5 s. Then, the central fixation spot disappeared and the monkeys were free to gaze anywhere they wished because reward would always be delivered; 50% of the trials were termed novelty-seeking trials (Fig. 1a, upper). During one half of these trials, one of two familiar objects appeared. These objects predicted the delivery of a novel object contingent on the animal behavior. That is, if the animals gazed at these peripheral familiar visual objects, they were immediately replaced by a novel object which remained on the screen until the outcome. We termed these NP object trials. During the other half of the novelty-seeking trials, one of two familiar objects was presented, and if the animal gazed at them, instead of a novel object, one of two familiar objects was shown. We termed these FP object trials. The task-timing and reward parameters of these two trial types were precisely the same. Another group of trials we termed novelty-inspecting trials (Fig. 1a, bottom). These constituted the other 50% of the trials. During these trials, the peripheral objects presented following trial start fixation were either novel (on half of the novelty-inspecting

trials) or one of two familiar objects. The novelty-seeking and inspecting trials were not blocked. So, in sum during novelty- inspecting and seeking trials, following the trial start fixation epoch, the animals experienced a novel object with 25% chance and a familiar object that could deliver a novel object (NP trials) with 25% chance.

A distinct group of trials began with a pink fixation spot. During these trials the monkeys experienced either a novel object (50%) or one of two familiar objects. However, the two novel objects used in these trials were not 'regenerated' during the experimental session. That is, they underwent novelty-familiarity transformations (learning) because the novel object remained the same and re-appeared throughout the recording session. These trials were used to gain additional evidence that novelty directly mediates gaze behavior. They also further tested whether the dopaminergic system differentiates novelty-familiarity. The timing and reward statistics of these trials were the same as the other trials described above.

In one sixth of trials, unpredicted rewards or unpredicted sensory events, termed unpredicted no-reward cues, were delivered during the ITI (ranging from 0.7 s to 1.5 s from ITI start). During a single ITI with an unpredicted event, the monkeys experienced only one type of ITI event (reward or no-reward cue).

We further verified monkeys' novelty preferences in a distinct choice task (Supplementary Fig. 2). Here, the animals chose between NP and FP objects (the same as in Fig. 1a in novelty-seeking trials). In this way the monkeys could choose to obtain a novel or familiar object. Reward was not dependent on whether the monkeys chose to receive familiar or novel objects. Hence, the task measured the monkeys' preference to obtain the opportunity to gaze at a novel object, not their preference for rewards.

Statistical analyses. All statistical tests are specified wherever *P* values are reported and were nonparametric and two sided unless otherwise noted. Correlations were Spearman's rank correlations. No statistical methods were used to predetermine sample sizes but our sample sizes are similar to those reported in previous studies in nonhuman primates^{35,52,57}. Data collection and analysis were not performed blind to the conditions of the experiments, without randomization procedures and were not excluded.

Fractal object acquisition time was defined as the time from when a central fixation spot disappeared to when an animal gazed at a peripheral fractal object and kept fixating it over 100 ms (5-degree window around fractal object). The proportion of free viewing spent gazing at an object was measured in the last 2 s before the outcome. In addition, trials in which fractal object acquisition occurred within this time window were removed from this analysis.

Significant task responsiveness was defined as variance in neural activity across all task events, including ITI events. To determine whether recorded neurons had significant task event-related modulations, we computed *P* values by comparing activities across different trial or event types within the time windows 50 to 350 ms from object onset, -200 to 100 ms from gaze object acquisition, and 100 to 400 ms from ITI events (Kruskal-Wallis test; *P* < 0.05). The windows were chosen such that they included key neuronal modulations in each area and were wide enough to avoid bias towards a particular response pattern (e.g., phasic versus tonic). The comparisons were done across ipsilateral and contralateral NP, FP, novel and familiar trials; and in the ITI window across unpredicted reward, unpredicted no-reward cue, and no-event ITI baseline activities. The *P* values were then combined^{91,92}. This nonparametric method has fewer assumptions than parametric methods. Nonetheless, we also cross-validated it by a general linear model approach which yielded similar key results for each brain area.

Neural activity was converted to normalized activity as follows. Each neuron's spiking activity was smoothed with a Gaussian kernel (mean = 50 ms, or 5 ms in Supplementary Fig. 8) and then *z*-scored. To *z*-score the activity, the neuron's average activity time course aligned at post fixation peripheral object onset was calculated for each condition. These average activity time courses from the different conditions were all concatenated into a single vector, and its mean and s.d. were calculated and used to *z*-score the data. Therefore, these analyses converted that neuron's firing rates to normalized activity by: (1) subtracting the mean of that vector; (2) dividing by the s.d. of that vector⁵⁷. To quantify the novelty-motivated object acquisition response-time bias (novelty bias), we created an index that was computed from the differences in object acquisition times:

$$A = \left(\overline{RT}_{FP} - \overline{RT}_{NP} \right) / \left(\overline{RT}_{FP} + \overline{RT}_{NP} \right)$$

$$B = \left(\overline{RT}_{Familiar} - \overline{RT}_{Novel} \right) / \left(\overline{RT}_{Familiar} + \overline{RT}_{Novel} \right)$$

$$\text{Novelty - bias index} = (\bar{A} + \bar{B}) / 2$$

where \overline{RT}_{NP} , \overline{RT}_{FP} , \overline{RT}_{novel} , $\overline{RT}_{familiar}$ indicate object acquisition times in NP, FP, novel and familiar trials, respectively. The index was computed separately for each session.

For semi-chronic array recording, to avoid the silencing of trends by statistical thresholds, we report the raw cell count numbers, and verify the results with MUA analyses. Because in ZI we found that novelty signals were correlated in

novelty-seeking and inspecting trials, we defined novelty-seeking neurons as those task-related cells that displayed novelty preference in both trial types (rank-sum test; *P* < 0.05) with the same coding sign (e.g., inhibited by novelty in both or excited by novelty in both). A neuron could be classified as novelty-seeking-related if it passed our criteria on either contralateral or ipsilateral trials to the recording site.

Across all experiments, to derive neural selectivity indices that measured the strength of discrimination among task events, we used ROC area (AUC) to distinguish spike counts across groups of trials (e.g., novel versus familiar; unpredicted reward versus unpredicted no-reward cue). For each index, we specified the precise temporal window and groups of trials being compared in the main text or figure legends. Significance was of these indices was measured with Wilcoxon rank-sum tests as previously⁵⁷.

Novelty signal latencies were derived as in other studies^{57,93,94}. These analyses were meant to assess the structure of neural activations in our task across different brain areas. Briefly for two groups of novelty trials (e.g., NP versus FP) we computed AUC in time, comparing spike density functions (SDFs) across the two conditions. Latency of discrimination was when the AUC was significantly greater than chance (0.5 AUC being chance; threshold: ≥ 0.6 for novelty excited, or ≤ 0.4 for novelty inhibited; *P* value threshold: 0.05) for at least 30 ms. The key advantage of this approach is that it accurately reflects the relative differences in latency across different brain regions⁹³, but like all analyses of latency, it does not index the precise true 'time' at which the brain explicitly has access to particular information to guide behavior. We performed this analysis including all task-related neurons in each brain area without other preselection. All neurons that yielded a latency were included.

Electrical stimulation and pharmacological inactivation. During electrical stimulation sessions, low-intensity electrical stimulation (50 uA, 400 Hz, 300 ms) was delivered from fractal onset on 50% of trials. The stimulation strength was chosen on the basis of previous studies in monkeys^{81,95,96}. Stimulation near the ZI did not facilitate saccades, suggesting that our stimulation parameters could have minimized current spread and off-target activation of fibers of passage as suggested by previous work^{81,96-98}. The stimulation sites in ZI were determined where significant novelty-excited neurons were found in single-unit recording. The stimulation sites in the subthalamic nucleus and the thalamus were determined to be ~1 or ~2 mm apart from stimulation sites in ZI along the electrode path. We also unilaterally injected the GABAa agonist muscimol (8 μg/μl for monkey R, 4 μg/μl for monkey S) into the ZI of monkeys R and S. The injection sites were determined where neurons showing a significant novelty-related activity were recorded in single-unit recording. The drug solution was pressure injected, 0.1 μl per minute at 1-min intervals (0.4 to 0.8 μl in total), using a 10-μl microsyringe (Hamilton) with a handmade injector. During each session, the monkeys first performed 250 trials as a preinjection control. The drug was then injected. Fifteen minutes after the injection, the monkeys started performing postinjection trials. We also conducted sham sessions (*n* = 4 in monkey R, and *n* = 13 in monkey S) as controls in which exactly the same procedures as those during the muscimol injection sessions were performed, but we did not place the injectrode into the brain. All shams were included. Repeating the analyses in Fig. 4a with the first six sham sessions for monkey S (to match the number of inactivation sessions) produced the same key results.

Reporting Summary. Further information on research design is available in the Nature Research Reporting Summary linked to this article.

Data availability

All data are available upon reasonable request from the corresponding author.

Code availability

All code is available upon request.

References

- Daye, P. M., Monosov, I. E., Hikosaka, O., Leopold, D. A. & Optican, L. M. pyElectrode: an open-source tool using structural MRI for electrode positioning and neuron mapping. *J. Neurosci. Methods* **213**, 123–131 (2013).
- Ledbetter, M. N., Chen, D. C. & Monosov, I. E. Multiple mechanisms for processing reward uncertainty in the primate basal forebrain. *J. Neurosci.* **36**, <https://doi.org/10.1523/JNEUROSCI.1123-16.2016> (2016).
- Dotson, N. M., Hoffman, S. J., Goodell, B. & Gray, C. M. A large-scale semi-chronic microdrive recording system for non-human primates. *Neuron* **96**, 769–782. e762 (2017).
- Dotson, N. M., Hoffman, S. J., Goodell, B. & Gray, C. M. Feature-based visual short-term memory is widely distributed and hierarchically organized. *Neuron* **99**, 215–226. e214 (2018).
- Monosov, I. E., Leopold, D. A. & Hikosaka, O. Neurons in the primate medial basal forebrain signal combined information about reward uncertainty, value, and punishment anticipation. *J. Neurosci.* **35**, 7443–7459 (2015).
- Yamamoto, S., Monosov, I. E., Yasuda, M. & Hikosaka, O. What and where information in the caudate tail guides saccades to visual objects. *J. Neurosci.* **32**, 11005–11016 (2012).

82. Monosov, I. E. & Hikosaka, O. Regionally distinct processing of rewards and punishments by the primate ventromedial prefrontal cortex. *J. Neurosci.* **32**, 10318–10330 (2012).
83. Mao, D. et al. Spatial representations in macaque hippocampal formation. *bioRxiv*, 2020.2010.2003.324848, <https://doi.org/10.1101/2020.10.03.324848> (2020).
84. Markov, N. T. et al. A weighted and directed interareal connectivity matrix for macaque cerebral cortex. *Cereb. Cortex* **24**, 17–36 (2014).
85. Ogasawara, T., Nejime, M., Takada, M. & Matsumoto, M. Primate nigrostriatal dopamine system regulates saccadic response inhibition. *Neuron* **100**, 1513–1526. e1514 (2018).
86. Ungless, M. A. & Grace, A. A. Are you or aren't you? Challenges associated with physiologically identifying dopamine neurons. *Trends Neurosci.* **35**, 422–430 (2012).
87. Ongur, D. & Price, J. L. The organization of networks within the orbital and medial prefrontal cortex of rats, monkeys and humans. *Cereb. Cortex* **10**, 206–219 (2000).
88. Carmichael, S. & Price, J. L. Limbic connections of the orbital and medial prefrontal cortex in macaque monkeys. *J. Comp. Neurol.* **363**, 615–641 (1995).
89. Carmichael, S. T., Clugnet, M. C. & Price, J. L. Central olfactory connections in the macaque monkey. *J. Comp. Neurol.* **346**, 403–434 (1994).
90. Kondo, H., Saleem, K. S. & Price, J. L. Differential connections of the temporal pole with the orbital and medial prefrontal networks in macaque monkeys. *J. Comp. Neurol.* **465**, 499–523 (2003).
91. Fisher, R. A. *Breakthroughs in Statistics* 66–70 (Springer, 1992).
92. Rolls, E. T. & Xiang, J.-Z. Reward-spatial view representations and learning in the primate hippocampus. *J. Neurosci.* **25**, 6167–6174 (2005).
93. Monosov, I. E., Trageser, J. C. & Thompson, K. G. Measurements of simultaneously recorded spiking activity and local field potentials suggest that spatial selection emerges in the frontal eye field. *Neuron* **57**, 614–625 (2008).
94. Monosov, I. E., Sheinberg, D. L. & Thompson, K. G. Paired neuron recordings in the prefrontal and inferotemporal cortices reveal that spatial selection precedes object identification during visual search. *Proc. Natl Acad. Sci. USA* **107**, 13105–13110 (2010).
95. Salzman, C. D. & Newsome, W. T. Neural mechanisms for forming a perceptual decision. *Science* **264**, 231–237 (1994).
96. Ballesta, S., Shi, W., Conen, K. E. & Padoa-Schioppa, C. Values encoded in orbitofrontal cortex are causally related to economic choices. *Nature* **588**, 450–453 (2020).
97. McIntyre, C. C. & Grill, W. M. Selective microstimulation of central nervous system neurons. *Ann. Biomed. Eng.* **28**, 219–233 (2000).
98. McIntyre, C. C. & Grill, W. M. Extracellular stimulation of central neurons: influence of stimulus waveform and frequency on neuronal output. *J. Neurophysiol.* **88**, 1592–1604 (2002).

Acknowledgements

This work is supported by the National Institute of Mental Health under award numbers R01MH110594 and R01MH116937 to IEM, and by the McKnight Foundation award to IEM. The optimization of array technology was supported by the Defense Advanced Research Projects Agency (DARPA) Biological Technologies Office (BTO) ElectRx program under the auspices of D. Weber through the CMO grant/contract no. HR0011-16-2-0022. We are grateful to K. Kocher for great animal care and animal training, and to A. Kepecs, E. S. Bromberg-Martin and C. Padoa-Schioppa for giving us valuable suggestions to improve this manuscript. We are also grateful to B. Goodell and C. M. Gray for technical and scientific assistance with high channel-count recording arrays, to D. W. Moran for assistance with perfusion, and to FD Neuro Technologies for assistance with tissue processing.

Author contributions

T.O., I.E.M. and Y.F. performed the neuronal recordings. T.O., F.S., K.Z. and J.P. analyzed the data. I.E.M. wrote the manuscript. T.O., J.P., Y.F. and I.E.M. discussed and revised the manuscript. A.J. analyzed the anatomical data. I.E.M. guided and conceptualized the research.

Competing interests

The authors declare no competing interests.

Additional information

Supplementary information The online version contains supplementary material available at <https://doi.org/10.1038/s41593-021-00950-1>.

Correspondence and requests for materials should be addressed to Takaya Ogasawara or Ilya E. Monosov.

Peer review information *Nature Neuroscience* thanks Mitsuko Watabe-Uchida and the other, anonymous, reviewer(s) for their contribution to the peer review of this work.

Reprints and permissions information is available at www.nature.com/reprints.

Reporting Summary

Nature Research wishes to improve the reproducibility of the work that we publish. This form provides structure for consistency and transparency in reporting. For further information on Nature Research policies, see our [Editorial Policies](#) and the [Editorial Policy Checklist](#).

Statistics

For all statistical analyses, confirm that the following items are present in the figure legend, table legend, main text, or Methods section.

- | | |
|-------------------------------------|--|
| n/a | Confirmed |
| <input type="checkbox"/> | <input checked="" type="checkbox"/> The exact sample size (n) for each experimental group/condition, given as a discrete number and unit of measurement |
| <input type="checkbox"/> | <input checked="" type="checkbox"/> A statement on whether measurements were taken from distinct samples or whether the same sample was measured repeatedly |
| <input type="checkbox"/> | <input checked="" type="checkbox"/> The statistical test(s) used AND whether they are one- or two-sided
<i>Only common tests should be described solely by name; describe more complex techniques in the Methods section.</i> |
| <input type="checkbox"/> | <input checked="" type="checkbox"/> A description of all covariates tested |
| <input type="checkbox"/> | <input checked="" type="checkbox"/> A description of any assumptions or corrections, such as tests of normality and adjustment for multiple comparisons |
| <input type="checkbox"/> | <input checked="" type="checkbox"/> A full description of the statistical parameters including central tendency (e.g. means) or other basic estimates (e.g. regression coefficient) AND variation (e.g. standard deviation) or associated estimates of uncertainty (e.g. confidence intervals) |
| <input type="checkbox"/> | <input checked="" type="checkbox"/> For null hypothesis testing, the test statistic (e.g. F , t , r) with confidence intervals, effect sizes, degrees of freedom and P value noted
<i>Give P values as exact values whenever suitable.</i> |
| <input checked="" type="checkbox"/> | <input type="checkbox"/> For Bayesian analysis, information on the choice of priors and Markov chain Monte Carlo settings |
| <input type="checkbox"/> | <input checked="" type="checkbox"/> For hierarchical and complex designs, identification of the appropriate level for tests and full reporting of outcomes |
| <input type="checkbox"/> | <input checked="" type="checkbox"/> Estimates of effect sizes (e.g. Cohen's d , Pearson's r), indicating how they were calculated |

Our web collection on [statistics for biologists](#) contains articles on many of the points above.

Software and code

Policy information about [availability of computer code](#)

Data collection: Collected with Plexon and Matlab Psychtoolbox. Described in methods

Data analysis: Analyzed with Custom Matlab scripts. MRI was visualized by PyElectrode. Kilosort2 was used for high channel data and then further processed by custom Matlab scripts. Offline sorting was also performed by Plexon Offline sorter.

For manuscripts utilizing custom algorithms or software that are central to the research but not yet described in published literature, software must be made available to editors and reviewers. We strongly encourage code deposition in a community repository (e.g. GitHub). See the Nature Research [guidelines for submitting code & software](#) for further information.

Data

Policy information about [availability of data](#)

All manuscripts must include a [data availability statement](#). This statement should provide the following information, where applicable:

- Accession codes, unique identifiers, or web links for publicly available datasets
- A list of figures that have associated raw data
- A description of any restrictions on data availability

Data will be made available upon request.

Field-specific reporting

Please select the one below that is the best fit for your research. If you are not sure, read the appropriate sections before making your selection.

Life sciences Behavioural & social sciences Ecological, evolutionary & environmental sciences

For a reference copy of the document with all sections, see [nature.com/documents/nr-reporting-summary-flat.pdf](https://www.nature.com/documents/nr-reporting-summary-flat.pdf)

Life sciences study design

All studies must disclose on these points even when the disclosure is negative.

Sample size	at least 2 animals for each electro physiological or behavioral study. this sample size is standard in NHP neurophysiology and was pre determined based on this standard
Data exclusions	none unless otherwise stated in methods or results
Replication	as is standard in our field, all key findings were replicated in at least 2 monkeys. all replications for key results were successful.
Randomization	N/A for behavioral and computational studies of NHP brain circuits.
Blinding	NHP neurophysiology is impossible to perform blind.

Reporting for specific materials, systems and methods

We require information from authors about some types of materials, experimental systems and methods used in many studies. Here, indicate whether each material, system or method listed is relevant to your study. If you are not sure if a list item applies to your research, read the appropriate section before selecting a response.

Materials & experimental systems

Methods

n/a	Involved in the study	n/a	Involved in the study
<input checked="" type="checkbox"/>	<input type="checkbox"/> Antibodies	<input checked="" type="checkbox"/>	<input type="checkbox"/> ChIP-seq
<input checked="" type="checkbox"/>	<input type="checkbox"/> Eukaryotic cell lines	<input checked="" type="checkbox"/>	<input type="checkbox"/> Flow cytometry
<input checked="" type="checkbox"/>	<input type="checkbox"/> Palaeontology and archaeology	<input type="checkbox"/>	<input checked="" type="checkbox"/> MRI-based neuroimaging
<input type="checkbox"/>	<input checked="" type="checkbox"/> Animals and other organisms		
<input checked="" type="checkbox"/>	<input type="checkbox"/> Human research participants		
<input checked="" type="checkbox"/>	<input type="checkbox"/> Clinical data		
<input checked="" type="checkbox"/>	<input type="checkbox"/> Dual use research of concern		

Animals and other organisms

Policy information about [studies involving animals](#); [ARRIVE guidelines](#) recommended for reporting animal research

Laboratory animals	Adult male rhesus monkeys (Macaca mulatta; ages 6-9 years old) were used for the electrophysiology experiments
Wild animals	No wild animals were used.
Field-collected samples	None
Ethics oversight	Approved by Washington University IACUC as well as USDA and NIH

Note that full information on the approval of the study protocol must also be provided in the manuscript.

Magnetic resonance imaging

Experimental design

Design type	MRI T1 images were acquired using a 3T magnet. This was not functional MRI.
Design specifications	This was not functional MRI. N/A
Behavioral performance measures	This was not functional MRI. N/A

Acquisition

Imaging type(s)	T1 images	
Field strength	3T	
Sequence & imaging parameters	Slice thickness of structural MRI = 0.5	
Area of acquisition	macaque brain	
Diffusion MRI	<input type="checkbox"/> Used	<input checked="" type="checkbox"/> Not used

Preprocessing

Preprocessing software	N/A
Normalization	N/A
Normalization template	N/A
Noise and artifact removal	N/A
Volume censoring	N/A

Statistical modeling & inference

Model type and settings	N/A
Effect(s) tested	N/A
Specify type of analysis:	<input checked="" type="checkbox"/> Whole brain <input type="checkbox"/> ROI-based <input type="checkbox"/> Both
Statistic type for inference (See Eklund et al. 2016)	N/A for structural MRI
Correction	N/A

Models & analysis

n/a	Involvement in the study
<input checked="" type="checkbox"/>	<input type="checkbox"/> Functional and/or effective connectivity
<input checked="" type="checkbox"/>	<input type="checkbox"/> Graph analysis
<input checked="" type="checkbox"/>	<input type="checkbox"/> Multivariate modeling or predictive analysis